Concurrent bioprinted scaffold with autologous bone and allogeneic BMSCs promote bone regeneration via recuiting native BMSCs

Yu Huan[1,2*], Hongqing Chen[1*], Dezhi Zhou[3,4*], Xin He[1*], Sanzhong Li[1], Xiuquan Wu[1], Bo Jia[1], Yanan Dou[1], Xiaowei Fei[1], Shuang Wu[1], Zhou Fei[1#], Tao Xu[3,4,5,6#], Fei Fei[7#]

1 Department of Neurosurgery, Xijing Hospital, Air Force Medical University, Xi'an, 710032, China.

2 Department of Neurosurgery, General Hospital of Northern Theater Command, Shenyang 110840, China.

3 Biomanufacturing and Rapid Forming Technology Key Laboratory of Beijing, Department of Mechanical Engineering, Tsinghua University, Beijing 100084, China.

4 Key Laboratory for Advanced Materials Processing Technology, Ministry of Education, Department of Mechanical Engineering, Tsinghua University, Beijing 100084, China.

5 Department of Precision Medicine and Healthcare, Tsinghua-Berkeley Shenzhen Institute, Shenzhen 518055, China.

6 Center for Bio-intelligent Manufacturing and Living Matter Bioprinting, Research Institute of Tsinghua University in Shenzhen, Shenzhen, 518057, China.

7 Department of Ophthalmology, Xijing Hospital, Air Force Medical University, Xi'an, 710032, China.

Preprint of Bio-Design and Manufacturing (unedited)

*These authors contributed equally to this work.

#Correspondence should be addressed to Fei Fei (feeplus@163.com), Tao Xu (xut@tsinghua-sz.org), and Zhou Fei (feizhou@fmmu.edu.cn).

Abstract

Autologous bone marrow-derived mesenchymal stem cells (BMSCs) have been shown to promote osteogenesis; however, whether allogeneic BMSCs (Allo-BMSCs) have effects on bone regeneration is not clear. Therefore, we explored the effect of Allo-BMSCs on promoting bone regeneration in 3D-printed autologous bone (AB) scaffolds. Firstly, we concurrently printed scaffolds with polycaprolactone, AB particles (ABP) and Allo-BMSCs for appropriate support, providing bioactive factors and seed cells to promote osteogenesis. *In vitro* studies showed that AB scaffolds promoted the osteogenic differentiation of Allo-BMSCs. *In vivo* studies revealed that implantation of scaffolds loaded with ABP and Allo-BMSCs into canine skull defects for 9 months promoted osteogenesis. Further studies suggested that only a small portion of implanted Allo-BMSCs survived and became the vascular endothelial cell, chondrocyte, and osteocyte, and the implanted Allo-BMSCs released stromal cell-derived factor 1 through paracrine signaling to recruit native BMSCs into the defect, promoting bone regeneration. This study provides additional opportunities for the future uses of Allo-BMSCs.

Preprint of Bio-Design and Manufacturing (unedited)

Graphical Abstract

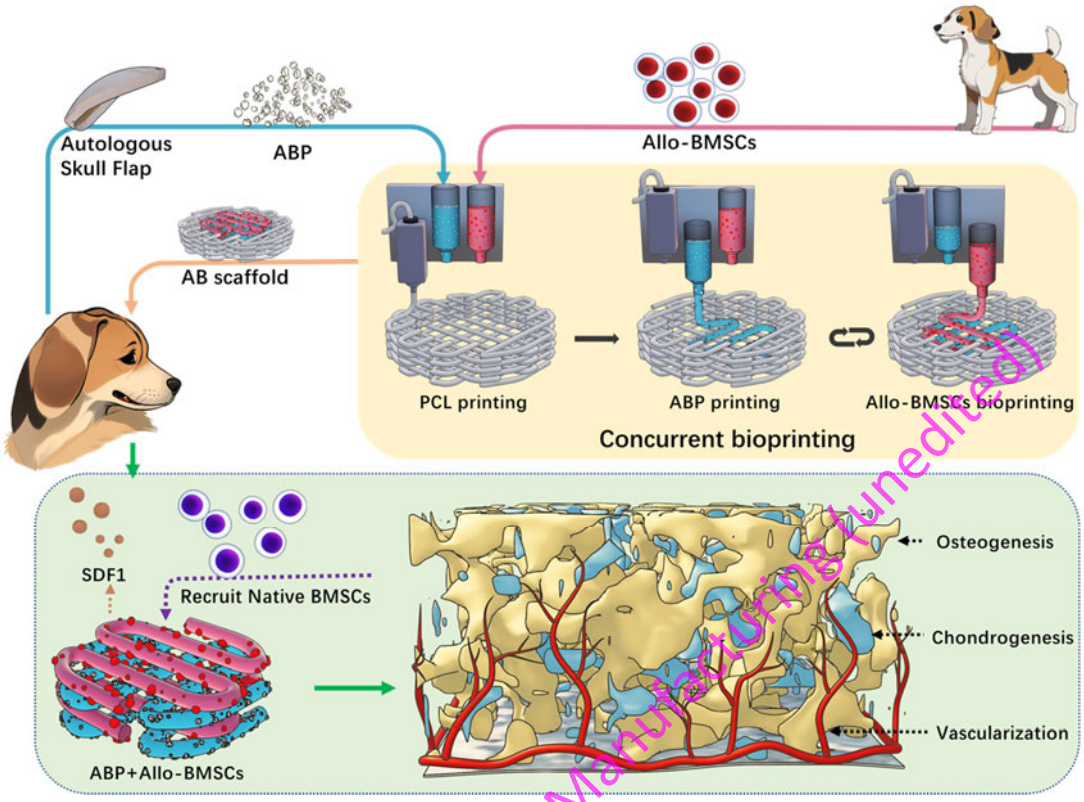

Preprint of Bio-Design and Manufacturing (unedited)

Keywords

concurrent 3D bioprinting, cranioplasty, autologous bone particles, allogeneic mesenchymal stem cells, recruitment

Introduction

Owing to various environmental factors, including the development of industries and transportation and the frequent occurrence of wars and terrorist activities, the incidence of head and craniofacial injuries has increased [1, 2]. Such injuries, along with related treatments such as decompressive craniectomy, may result in various cranial and facial bone defects, which, in turn, may have a range of consequences. These consequences include impaired recovery of brain

function, development of psychophysical disorders, and imposition of socio-economic burdens [3, 4]. In such cases, successful cranioplasty is critical [5].

Autologous bone (AB) grafting has traditionally been considered the ideal method for cranioplasty [6]. We previously tested a 3D-printed AB particles (ABP) scaffold with autologous bone marrow-derived mesenchymal stem cells (Auto-BMSCs). The scaffold demonstrated an ability to promote osteogenesis, offering a potential solution to address bone flap absorption during AB grafting [7, 8]. However, in clinical practice, Auto-BMSCs cannot be obtained through bone puncture owing to bone marrow senescence, hematopoietic system diseases, and so on. In such cases, allogeneic BMSCs (Allo-BMSCs) may be a viable alternative [9, 10]. However, whether Allo-BMSCs are viable alternative options within 3D-printed AB scaffolds remains unknown. To this end, we studied 3D-printed AB scaffolds loaded with Allo-BMSCs and verified their bone regeneration capacity. In this study, polycaprolactone (PCL) was applied to provide support, the AB stored in the -80℃ condition could release the bioactive factors to promote osteoinduction, Allo-BMSCs was used as the seed cells for osteogenesis. In this concurrent printing system, PCL, ABP and Allo-BMSCs were concurrently printed into a staggered scaffold to develop the strength and bone regenerative potential. In short, we designed a novel concurrent bioprinted scaffold containing natural materials and explore its potential of promoting bone regeneration.

Preprint of Bio-Design and Manufacturing (unedited)

Materials and Methods

1. Animals

Male Beagle dogs (age, 18–20 months old; weight, 15–18 kg) were purchased from Dilepu Biomedical Co., Ltd. (Xi'an, China; license number SCXK 2019-002). All experimental animal handling procedures were performed in accordance with the Chinese Animal Experimentation

Law and were approved by the Ethics Committee of Air Force Medical University (Xi'an, China; approval number IACUC-20210120). All animals were housed in a room (temperature 25±1°C, humidity 40–70%, 12 h light/dark cycle) with *ad libitum* access to food and water.

2. Modeling and grouping

A full-layer skull defect model, measuring 2 cm in diameter, was made on the right side 2.5 cm away from the sagittal suture and 2.5 cm behind the anterior fontanel. Following this, the skull flap was sampled and kept at -80°C, and ground into ABP before use. Three months later, the cranioplasty was performed. In this experiment, a concurrent bioprinting was used bedside [7]. Briefly, the scaffold loaded with ABP and Allo-BMSCs was printed concurrently at the bedside and immediately used for cranioplasty. Cranioplasty materials from different groups were implanted and fixed with sutures. Animals were sacrificed either 3 or 9 months after cranioplasty, and each transplanted skull was cleaned and fixed with 4% paraformaldehyde for examination.

In vivo and *in vitro* methods were used in this study. *In vitro* studies were divided into 2D and 3D experiments, in which the same conditions were used for both culture systems with the exception that scaffolds were not used in the 2D culture systems. Both the 2D and 3D experiments fell into three groups (Allo, ABP/Allo, and nano-hydroxyapatite [nHA]/Allo) according to the varying compositions of the culture systems. For the *in vivo* studies, dogs were randomized into four groups (3 dogs/group) as follows: 1) cranioplasty with a PCL scaffold (PCLS); 2) cranioplasty with a PCLS and Allo-BMSCs scaffold (PCLS/Allo); 3) cranioplasty with a PCLS, ABP, and Allo-BMSCs scaffold (PCLS/ABP/Allo); and 4) cranioplasty with a PCLS, nHA, and Allo-BMSCs scaffold (PCLS/nHA/Allo).

3. *Scaffold preparation*

Preprint of Bio-Design and Manufacturing (unedited)

1) Allo-BMSCs preparation

Allo-BMSCs were isolated as previously described [8]. Briefly, 8 mL of bone marrow blood was collected from the another dog‘s femur and added into Histopaque-1077 (10771, Sigma Diagnostics, MO, USA) to isolate the BMSCs [10]. Primary BMSCs were cultured in the incubator (37°C, 5% CO_2) until the third generation for the following experiments.

2) ABP preparation

ABP were prepared according to previously published protocols [9]. Briefly, the skull flaps were crushed, dialyzed, and lyophilized (-80°C, 1 Pa) for 24 h (LYOQUEST-85, Telstar, Spain), and then were ground into ABP by a vibration grinder (GRINDER GT200, Beijing Grinder Instrument Co., Ltd., China).

3）Bioink preparation and concurrent 3D printing

Ink preparation and 3D printing were performed as previously described [8]. The BMSCs and ABP bioink was composed of a cell suspension containing 25% AB solution, 10% gelatin solution, and 2% sodium alginate solution [8]. A multinozzle bioprinter (Livprint Norm, MedPrin, China) was used for concurrent bio-printing. Briefly, after printing PCL into a shell, AB and Allo-BMSCs were printed layer by layer in a staggered manner inside the shell, our implanted scaffolds were 20 × 20 × 2.1 mm multi-tiered square grids (Fig. 1b).

4. Examinations

1) Scanning-electron microscopy (SEM)

All scaffolds were fixed and dehydrated. SEM was used to observe the scaffolds and capture cell images. Scaffolds were fixed using 2.5% glutaraldehyde and dehydrated using gradient alcohol. After vacuum drying, the samples were sprayed with Pt, and cell images were captured using

Preprint of Bio-Design and Manufacturing (unedited)

SEM (S4800, HITACHI, Japan). The software was the system software of S4800 HITACHI SEM.

2) Quantitative real-time polymerase chain reaction (PCR) analysis

PCR testing was used to observe the relative expression of osteogenic mRNA. The primers of quantitative real-time PCR used in this experiment are shown in Supplementary Table 1, and glyceraldehyde 3-phosphate dehydrogenase (GAPDH) was evaluated as the reference gene.

3) Alkaline phosphatase (ALP)-activity detection

ALP activity was examined according to the manufacturer's instructions to evaluate osteogenic differentiation (P0321S, Beyotime, China). After the BMSCs were collected by dissolving scaffolds in the mixed solution (55 mM sodium citrate, 20 mM EDTA), they were incubated in a detection buffer (reagent in the kit) at 37℃ for 10 min. Finally, ALP activity was calculated by observing the absorbance at 405 nm.

4) Micro-computed tomography (Micro-CT) assay

To evaluate bone regeneration, bone specimens in all groups were scanned and imaged using a micro-CT system (ZKKS-MCT-Sharp, China). Reconstruction and analysis were performed using isotropic 20 μm voxels with the ZKKS-Micro-CT 3.0 instrument (ZKKS, China), and further analysis was performed with the ZKKS-Micro-CT 4.1 software (ZKKS, China). The scan was performed 1.0 cm around the perimeter of the skull defect, and the implanted area with a diameter of 2.0 cm was further analyzed and considered as the region of interest (ROI). To quantify the results of micro-CT, the bone volume per tissue volume (BV/TV) was recorded. The characteristics of trabecular bone, including trabecular number (Tb.N) and trabecular spacing (Tb.Sp), were statistically analyzed.

5) Histology and immunohistochemistry

Preprint of Bio-Design and Manufacturing (unedited)

Bone regeneration was assessed by histological staining and immunohistochemistry. For immunohistochemistry, antibodies against ossification marker such as collagen I (Col1, ab6308, Abcam, UK, 1:1000) and osteocalcin (OCN, MAB1419, R&D Systems, USA, 1:1000); cartilage marker such as collagen II (Col2, ab34712, Abcam, 1:1000) and aggrecan (Acan, ab36861, Abcam, 1:1000) were applied and incubated for 16-20 h. For the immunofluorescence study, antibodies against cluster of differentiation 31 (CD31, 11265-1-AP, Proteintech, China, 1:1000), Col1, Col2, CD105 (ab156756, Abcam, 1:1000), CD90 (ab92574, Abcam, 1:1000), and stromal cell-derived factor 1 (SDF1, 17402-1-AP, Proteintech, 1:1000) were applied and incubated for 16-20 h. Immunostained images were captured by a fluorescence microscope (FV10i; Olympus, Japan). The integral optical density per unit area (IOD/area) was measured by Image J software. And the positive cell number and relative fluorescence intensity were also measured by Image J software. Hematoxylin-eosin (HE), Masson's trichrome, and Safranin O-Fast Green staining were performed on the sections according to the instructions (G1120; G1340; G1371, Solarbio, China).

6) *Enzyme-linked immunosorbent assay (ELISA) testing*

We performed an ELISA test to study the changes in SDF1, a small protein with a crucial role in directing cellular migration [11], following the protocol outlined in the SDF1 ELISA Kit (KE10049, Proteintech).

5. In-vitro experiments

1) ALP staining

After remoting the culture medium, BMSCs in the dish were washed by PBS buffer for 3 times. The process of staining was performed as the instructions (G1480, Solarbio, China). In short, the cells were fixed with 4℃ ALP fixation fluid for 1 min. After distilled water

Preprint of Bio-Design and Manufacturing (unedited)

washing, the cells were incubated with ALP solution for 15min in 37℃.

2) ALP activity detection

After printing, the scaffolds were cultured in an osteogenic induction medium for 2 weeks and dissolved in 55 mM trisodium citrate and 20 mM ethylene diamine tetra-acetic acid (EDTA). After the cells encapsulated in the scaffold extraction, the ALP activity detection was performed as the instrument (P0321S, Beyotime, China).

3) Co-culture system

The co-culture system was performed by transwell insert. The BMSCs were cultured in the upper chamber, and the scaffolds were cultured in the lower chamber.

4) SDF1 detection

The SDF1 detection was conducted by the kit (KE10049, Proteintech, China). In short, the culture medium supernatant and reference standard were added into the ELISA plate. After incubation for 2h in 37℃, the plate was washed by washing buffer for 4 times. The testing solution was added and incubated for 1h in 37℃. After washing for 4 times, the HRP solution was added and incubated for 40min in 37℃. After washing for 4 times, the TMB solution was added and incubated for 15min in 37℃ from light. After addition of stopping buffer, the plate was further measured and calculated.

5) Migration detection

The BMSCs were cultured in the upper chamber of transwell, while the scaffolds were culture in the lower chamber. After 24h co-culture, the BMSCs staying in the upper chamber of the transwell were gently erased, and then crystal violet staining was used to detect the BMSCs that micgrated to the backside of the transwell membrane.

Preprint of Bio-Design and Manufacturing (unedited)

6. Statistical analysis

All experiments were performed in at least triplicate, and all results are presented as the mean ± the standard error of the mean. Differences were analyzed by a one-way analysis of variance (ANOVA) with the Tukey's post hoc test via GraphPad Prism 8 (GraphPad Software, USA). $P < 0.05$ was considered statistically significant.

Preprint of Bio-Design and Manufacturing (unedited)

Results

1. Morphological manifestations of concurrent bioprinted scaffolds

PCL, ABP, and Allo bioinks were printed onto a multilayer composite scaffold with a diameter of 2 cm (Fig. 1 a and 1 b). The ABP, Allo, and nHA grids were clearly observed under a light microscope (Fig. 1 c). The SEM analysis revealed that the Allo-BMSCs were encapsulated in the bioink and protruded from the surface (Fig. 1 d), similar to the results of our previous study [8]. The nHA and ABP particles formed uneven, porous surfaces on the scaffolds to facilitate cell adhesion (Fig. 1 d), and the cell viability of ABP/Allo scaffold was tested (Supplemental Fig. 1). The results showed that the scaffolds possessed good cellular affinity. And ABP particle was mainly 92 μm in size (Supplemental Fig. 2).

2. Role of Allo-BMSCs in osteogenic differentiation in vitro

The *in vitro* effects of ABP and nHA on osteogenic differentiation were evaluated, and the experimental design is shown in Fig. 2 a. ALP staining revealed that although both ABP and nHA played a role in promoting osteogenic differentiation of Allo-BMSCs, ABP was more effective (Fig. 2 b). This was confirmed by PCR using a 2D culture system (Fig. 2 c). When Allo, ABP/Allo, and nHA/Allo hybrid scaffolds were used in the 3D culture system (Fig. 3 a), the ALP activity in

the ABP/Allo group was higher than that in the Allo and nHA/Allo groups (Fig. 3 b). In addition, the expression of osteogenesis-related mRNA such as OCN, BMP2, and RUNX2, showed a trend similar to that of ALP activity (Fig. 3c), verifying the ability of Allo-BMSCs to promote osteogenesis in the ABP/Allo scaffold.

3. Role of Allo-BMSCs in osteogenic differentiation in vivo

Three months after cranioplasty, the PCLS/ABP/Allo group had a higher collagen volume, indicating that Allo-BMSCs were present in the scaffolds and ABP had better potential for bone regeneration *in vivo*. The PCLS/Allo, PCLS/ABP/Allo, and PCLS/nHA/Allo groups had higher expression levels of Acan and Col2 than that in the PCLS group, with the PCLS/ABP/Allo group showing the highest expression of ABP (Fig. 5), suggesting the capability of ABP combined with Allo-BMSCs to promote chondrogenesis. We also found that Allo-BMSCs and ABP exerted effects on Col1 expression but had no effect on OCN expression (Fig. 5). Immunohistochemical staining of OCN and Col1 showed a similar trend, demonstrating that the osteogenesis promotion capabilities of Allo-BMSCs and ABP scaffolds were superior to those of PCLS/Allo and PCLS/nHA/Allo scaffolds.

Next, 9 months after cranioplasty, using HE, Masson, and Safranin O-Fast Green staining methods, light and dark red osteoid structures were observed and confirmed to be immature osteoid structures in the PCLS group (Fig. 6). In the PCLS/Allo group, except for the mature osteoid structures in the cranial defects, no mature bone tissue could be seen. In the PCLS/nHA/Allo group, the local red bone tissue was confirmed to be mature bone tissue (Fig. 6). In the PCLS/ABP/Allo group, new bone was found with more mature tissues at the surface and in deeper structures (Fig. 6). Representative micro-CT images are shown in Fig. 7a.

Preprint of Bio-Design and Manufacturing (unedited)

The finding that the BV/TV were similar in the PCLS/Allo and PCLS groups but were lower than those in the PCLS/ABP/Allo and PCLS/nHA/Allo groups suggests that ABP and nHA have potential for promoting osteogenesis (Fig. 7b). Further, the higher relative bone volume fractions in the PCLS/ABP/Allo group than that in the PCLS/nHA/Allo group suggests the osteogenesis-promoting ability of ABP (Fig. 7b). The Tb.N and Tb.Sp differences among groups were consistent with the results of the BV/TV (Fig. 7c-d), indicating that the PCLS/ABP/Allo scaffolds had better effects on bone regeneration.

4. Possible roles of Allo-BMSCs in scaffolds for bone regeneration

1) Roles of Allo-BMSCs in scaffolds in the differentiation of different tissues

To monitor and observe the transplanted BMSCs, Allo-BMSCs were pre-transfected with green fluorescent protein (GFP) before scaffold transplantation and examined 9 months after cranioplasty. The PCLS/Allo group had more CD31- and GFP-positive cells than that of the PCLS group, and several GFP-labeled Allo-BMSCs became CD31-positive (Fig. 8). In the PCLS/ABP/Allo and PCLS/nHA/Allo groups, more Allo-BMSCs survived and became CD31-positive than those in the PCLS/Allo group. To determine whether the implanted BMSCs became bone tissue, Col1 and GFP were co-stained. In the PCLS/Allo group, few GFP-labeled cells were detected in Col1 positive-stained regions, revealing that while Allo-BMSCs underwent the process of osteogenic differentiation and produced new bones, a part of new bones was not produced from the implanted Allo-BMSCs (Fig. 9). The PCLS/ABP/Allo group had more Col1-positive cells than the PCLS/Allo and PCLS/nHA/Allo groups, indicating that ABP boosted osteogenic BMSC differentiation. To verify whether Allo-BMSCs could transform into Col2-positive chondrocytes, Col2 was co-stained with GFP (Fig. 10). We found that several

Preprint of Bio-Design and Manufacturing (unedited)

chondrocytes from GFP-labeled BMSCs were present in the PCLS/ABP/Allo group, suggesting that chondrogenesis was facilitated in the PCLS/ABP/Allo group (Fig. 10).

2) Allo-BMSCs and ABP jointly *recruited native BMSCs*

To ascertain whether the scaffolds could recruit native stem cells, BMSCs were co-stained with the stem cell markers CD90 and CD105. Compared with the PCLS/Allo and PCLS/nHA/Allo groups, the PCLS/ABP/Allo group recruited more native stem cells around the GFP+ cells (Fig. 11), revealing that ABP and Allo-BMSCs synergistically promoted the recruitment of native stem cells. Moreover, SDF1 expression increased with the addition of Allo-BMSCs and ABP (Fig. 12 a). It is hypothesized that scaffolds containing Allo-BMSCs and ABP may promote the *in vivo* expression of SDF1 and recruitment of native stem cells. This was confirmed by our *in vitro* co-culture study, in which the Allo, ABP/Allo, or nHA/Allo scaffolds were placed in the lower transwell chamber and BMSCs in the upper transwell chamber. When ABP was added to the 3D culture system, the SDF1 expression increased (Fig. 12 c), which facilitated the migration of BMSCs from the upper to the lower transwell chamber. The migration of BMSCs in the ABP/Allo group was greater than that in the Allo and nHA/Allo groups, indicating that the addition of ABP resulted in enhanced migration of BMSCs (Fig. 12 d). In addition, we evaluated the immune inflammation situation. The results of anti-inflammatory cytokines (IL-10, IL-4) immunofluorescence demonstrated that the addition of Allo-BMSCs wound not decrease the expression of IL-10 and IL-4 (Fig. 13). Meanwhile, the expression of pro-inflammatory cytokines (TNF-α, IL-1β) in PCLS/Allo, PCLS/ABP/Allo, and PCLS/nHA/Allo was similar with that in PCLS group (Fig. 13), indicating that Allo-BMSCs in the scaffolds wound not aggravate inflammation in the bone defect area.

Preprint of Bio-Design and Manufacturing (unedited)

Discussion

In this study, we further investigated the efficacy and molecular mechanisms of Allo-BMSCs in a 3D-printed AB scaffold. First, *in vitro* experiments revealed that ABP promoted the osteogenesis of Allo-BMSCs. Therefore, scaffolds loaded with ABP and Allo-BMSCs (the PCLS/ABP/Allo group) were used for *in vivo* experiments. Immunohistochemical staining showed that the PCLS/ABP/Allo scaffolds promoted osteogenesis and chondrogenesis in the early stages. Long-term staining and micro-CT confirmed that the PCLS/ABP/Allo scaffolds could promote bone regeneration in the long term. Additionally, we stained Allo-BMSCs with GFP prior to cranioplasty and found that some Allo-BMSCs became cartilage and bone. GFP/CD90/CD105 co-staining revealed that many native BMSCs were recruited around the implanted Allo-BMSCs, demonstrating that the paracrine effects of Allo-BMSCs and native recruitment of BMSCs may be the molecular mechanism underlying bone regeneration. Finally, SDF1 detection and *in vitro* experiments demonstrated that the PCLS/ABP/Allo scaffolds promoted bone regeneration by releasing SDF1 and recruiting native BMSCs. Compared to single PCL, mixing PCL and particulate matter for printing will reduce the strength of the scaffold. In our previous study, we established a 3D-printed PCL/ABP scaffold to explore the effect of promoting bone regeneration, but the overall strength only reached the level of cancellous bone[7]. On the other hand, after ABP is encapsulated in PCL, due to the slow degradation of PCL, ABP cannot be engaged in the osteogenic environment as soon as possible, which limits its osteoinductive effect. Therefore, we designed this concurrent bioprinted scaffold to maintain the physical strength of PCL while ensuring sufficient contact between ABP, seed cells, and recipient tissue to fully exert the

Preprint of Bio-Design and Manufacturing (unedited)

osteogenic effect of the scaffold.

For hard tissue engineering applications, 3D printed biodegradable composite scaffolds have been extensively investigated[12]. Among these, PCL is extensively used in hard tissue engineering because of its unique physical strength. It was reported that a stable biphasic calcium phosphate (BCP)/PCL scaffold could promote sufficient proliferation and differentiation of pre-osteoblast cells[13]. Additionally, PCL combined with nano-hydroxyapatite, the inorganic component of bone tissue, showed great ability of bone regeneration[7, 14]. Owing to the good biocompatibility, sodium alginate-based material was widely used in tissue engineering, especially the cell loading scaffold[15]. Therefore, we combined the advantages of PCL and sodium alginate-based material to manufacture the 3D-printed ABP scaffolds in this study. Although it has previously been reported that 3D-printed ABP scaffolds loaded with Auto-BMSCs could promote bone regeneration [8], in daily clinical work, Auto-BMSCs are not available for many indications due to various disease contraindications in some patients. In addition, Auto-BMSCs are not suitable for older adult patients as aging has been reported to drive intrinsic changes in BMSCs, including reduced proliferation and osteogenic differentiation ability [16]. Therefore, there is a need to investigate the feasibility and role of Allo-BMSCs within a 3D-printed ABP scaffold. ABP was the complete extracellular matrix of bone tissues, including the organic and inorganic components. And the hydroxyapatite was the main crystalline form of calcium phosphate, composing the inorganic component of bone tissue. Previous studies revealed that hydroxyapatite possesses great osteoconductive function and is widely used in bone tissue engineering[17]. In the process of alveolar bone atrophy therapy, it was found that bone particles could promote the bone regeneration and showed osteogenic potential[18]. Therefore, the bone particles were considered

Preprint of Bio-Design and Manufacturing (unedited)

as the ideal material of bone tissue engineering[19]. Different with nHA, ABP might have better osteoconductive and osteoinductive properties. But the further mechanism of ABP promoting osteogenesis was still unclear, the most efficient component of bone particles organic components in osteogenesis needed further investigation.

Several studies have reported the protective capacity of Allo-BMSCs. Allo-BMSCs may have an important influence on the treatment of acute myocardial infarction and periodontitis and the promotion of muscle regeneration in preclinical studies [20-23]. After implantation, Allo-BMSCs can survive in brain and heart tissues and exert their effects over time [20, 21]. Local injection of Allo-BMSCs can inhibit inflammation in periodontitis tissue and promote periodontal tissue regeneration [22]. However, the immunogenic influence of Allo-BMSCs is a consideration for the application of Allo-BMSC implantation. In a Beagle dog model of critical-sized mandibular defects, though Allo-BMSCs manifested immune responses in the early stage, long-term bone regeneration was not influenced [24], confirming the safety of Allo-BMSC implantation in tissue-engineered bones. In our previous study, we manufactured the similar 3D printed scaffold with Auto-BMSCs[8]. Compared with this study, the area of new bone tissues in Auto-BMSCs scaffold was larger than that in Allo-BMSCs, indicating that Auto-BMSCs might be the better seed cell of bone tissue engineering. However, there are many limitations of Auto-BMSCs usage in clinical practice such as for the elderly or hematological disease patients. The aim of this study is trying to explore the possibility that Allo-BMSCs could replace Auto-BMSCs. Combined with our previous study, it is suggested that Allo-BMSCs might be the possible alternative option of seed cell for bone regeneration. More strategies including engineering stem cells and gene editing may provide a wider development space for Allo-BMSCs. Our study showed the immune response of

Preprint of Bio-Design and Manufacturing (unedited)

Allo-BMSCs scaffold in the long term was similar with that of PCLS scaffold, clarifying the safe and reliable characteristic of Allo-BMSCs in the bone tissue engineering. And the expression of pro-inflammatory factors in PCLS/ABP/Allo group was similar with that in PCLS group, indicating that the PCLS/ABP/Allo scaffold we designed would not aggravate the Immune inflammatory response. There was also a research investigating the osteogenic potential and immune response of Auto-BMSCs and Allo-BMSCs in the Lewis rat cranium defect model, in which the Allo-BSMCs elicited a weak immune response on day 14 that progressively attenuated by day 28[25]. It was also shown that Allo-BMSCs scaffold exhibited transient immune responses in the first 2 weeks post-implantation of beagle dogs critical-sized mandibular defect[24]. Meanwhile, the early immune response might influence the osteogenesis in the early term but not influence the long term[24, 25]. And it was indicated that Allo-BMSCs do not induce dendritic cell maturation, adding evidence to low immune response of Allo-BMSCs.

In vitro experiments have revealed the therapeutic potential of Allo-BMSC implantation [26]. However, the molecular mechanism of BMSC action in tissue-engineered bones remains controversial. The mainstream view is that BMSCs mainly promote bone regeneration via paracrine signaling and the release of bioactive factors rather than *in situ* differentiation of BMSCs [27]. In this study, we found that, compared with Auto-BMSCs, only some Allo-BMSCs could survive and differentiate into vascular endothelial cells, osteocytes, and chondrocytes. This suggests that Allo-BMSCs are sensitive to immune responses. Nevertheless, several native BMSCs surrounded the GFP-labeled Allo-BMSCs, demonstrating that the PCLS/ABP/Allo scaffolds promoted bone regeneration by releasing SDF1 and recruiting native BMSCs.

Preprint of Bio-Design and Manufacturing (unedited)

In bone tissue engineering, autologous material was found to be most useful for tissue repair [8, 28]. In tendon-to-bone healing, local delivery of fresh Auto-BMSCs was more efficacious than that of Allo-BMSCs [29]. In our previous study, ABP scaffolds loaded with Auto-BMSCs showed excellent bone-regeneration effects [8]. However, Allo-BMSCs may act as an alternative option. Bone-defect reconstruction may greatly benefit from the use of an allograft, which can serve as an invaluable adjunct material when combined with other materials [28]. It is known that at least 3 months are needed to evaluate bone regeneration, and the recommended observation period is 6 months after implantation. However, the remodeling process of woven bone into lamellar bone takes 6-12 months, which is accompanied by the absorption of native bone[30]. Clinical studies have shown that there is no statistical difference in loss of native bone after 9 months[31]. Furthermore, the cortical bone remodeling in dog bone regeneration was completed at 9 months[30]. Given this, we chose 9 months as the observation endpoint.

With the development of tissue engineering, single materials are gradually being replaced by composite materials. The present study proved that ABP can help Allo-BMSCs promote osteogenic differentiation, which was evidenced by a stronger osteogenic effect in the 3D culture system over the 2D culture system. Our *in vivo* study further indicated that ABP can help Allo-BMSCs promote osteogenesis, release SDF1, and recruit native BMSCs compared to PCLS/Allo and PCLS/nHA/Allo. Most importantly, with the assistance of ABP, the effect of Allo-BMSCs on SDF1 and the recruitment of native BMSCs may be key mechanisms. This provides a strategy for recruiting native BMSCs for muscle, endometrial, and craniofacial bone regeneration [23, 25, 32]. We believe that in future clinical applications, when bioactive factors of ABP are partially damaged owing to extended low-temperature storage, ABP combined with

Preprint of Bio-Design and Manufacturing (unedited)

Allo-BMSCs may synergistically promote *in situ* bone regeneration. SDF1 is the main chemokine that mediates the recruitment of BMSCs [33]. Moreover, recent studies have revealed that different types of stem cells can secrete various chemokines, including SDF1, to mediate cell migration [33, 34]. These studies provide theoretical support suggesting that Allo-BMSCs release SDF1 via paracrine signaling and recruit native BMSCs for bone regeneration.

This study has some limitations. First, the roles of Auto- and Allo-BMSCs were not compared in a single study. Second, the roles of Allo-BMSCs and ABP should be validated in more bioactive scaffolds. Other applications, such as coating and local injection, should also be explored. Furthermore, this study only explored the feasibility of using Allo-BMSCs to promote bone regeneration. In future studies, other methods such as the application of Allo-BMSC exosomes in bone regeneration can be explored.

Conclusions

Firstly, a novel concurrent bioprinted scaffold loaded with natural materials including bone particles and BMSCs was conducted and investigated for the bone regeneration potential. And we studied the role of Allo-BMSCs in a 3D-printed ABP scaffold using both an *in vitro* and i*n vivo* approach and found that scaffolds with ABP and Allo-BMSCs had the ability to promote osteogenesis. Further *in vivo* studies suggested that some of the implanted Allo-BMSCs survived and changed into vascular endothelial cell, chondrocyte, and osteocyte. Finally, the implanted Allo-BMSCs released SDF1 in a paracrine manner to recruit native BMSCs into the defect, promoting bone regeneration.

References

Preprint of Bio-Design and Manufacturing (unedited)

[1] Song, H., L. Konan, J. Cui, et al., *Nanometer ultrastructural brain damage following low intensity primary blast wave exposure*[J]. Neural Regeneration Research, 2018. **13**(9): p. 1516-1519.

[2] Rutter, B., H. Song, R.G. DePalma, et al., *Shock wave physics as eelated to primary non-impact blast-induced traumatic brain injury*[J]. Military Medicine, 2021. **186**(Supplement_1): p. 601-609.

[3] Chelly, H., M. Bahloul, R. Ammar, et al., *Clinical characteristics and prognosis of traumatic head injury following road traffic accidents admitted in ICU "analysis of 694 cases"*[J]. European Journal of Trauma and Emergency Surgery, 2017. **45**(2): p. 245-253.

[4] Alkhaibary, A., A. Alharbi, N. Alnefaie, et al., *Cranioplasty: a comprehensive review of the history, materials, surgical aspects, and complications*[J]. World Neurosurgery, 2020. **139**: p. 445-452.

[5] Shahid, A.H., M. Mohanty, N. Singla, et al., *The effect of cranioplasty following decompressive craniectomy on cerebral blood perfusion, neurological, and cognitive outcome*[J]. Journal of Neurosurgery, 2018. **128**(1): p. 229-235.

[6] Korhonen, T.K., J.P. Posti, J. Niinimäki, et al., *Two-center validation of the Oulu resorption score for bone flap resorption after autologous cranioplasty*[J]. Clinical Neurology and Neurosurgery, 2022. **212**: p. 107083.

[7] Chen, H., J. Zhang, X. Li, et al., *Multi-level customized 3D printing for autogenous implants in skull tissue engineering*[J]. Biofabrication, 2019. **11**(4): p. 045007.

[8] Huan, Y., D. Zhou, X. Wu, et al., *3D bioprinted autologous bone particle scaffolds for cranioplasty promote bone regeneration with both implanted and native BMSCs*[J]. Biofabrication, 2023. **15**(2).

[9] Wang, Z., L. Han, T. Sun, et al., *Extracellular matrix derived from allogenic decellularized bone marrow mesenchymal stem cell sheets for the reconstruction of osteochondral defects in rabbits*[J]. Acta Biomater, 2020. **118**: p. 54-68.

[10] Shokati, A., A. Naser Moghadasi, M. Nikbakht, et al., *A focus on allogeneic mesenchymal stromal cells as a versatile therapeutic tool for treating multiple sclerosis*[J]. Stem Cell Research & Therapy, 2021. **12**(1): p. 400.

[11] Ma, S., J. Zhou, T. Huang, et al., *Sodium alginate/collagen/stromal cell-derived factor-1 neural scaffold loaded with BMSCs promotes neurological function recovery after traumatic brain injury*[J]. Acta Biomaterialia, 2021. **131**: p. 185-197.

[12] Jang, T.S., S.J. Park, J.E. Lee, et al., *Topography-Supported Nanoarchitectonics of Hybrid Scaffold for Systematically Modulated Bone Regeneration and Remodeling*[J]. Advanced Functional Materials, 2022. **32**(51).

[13] Ahn, J.-H., J. Kim, G. Han, et al., *3D-printed biodegradable composite scaffolds with significantly enhanced mechanical properties via the combination of binder jetting and capillary rise infiltration process*[J]. Additive Manufacturing, 2021. **41**.

[14] Zimmerling, A., Z. Yazdanpanah, D.M.L. Cooper, et al., *3D printing PCL/nHA bone scaffolds: exploring the influence of material synthesis techniques*[J]. Biomaterials Research, 2021. **25**(1).

[15] Kim, N., H. Lee, G. Han, et al., *3D-Printed Functional Hydrogel by DNA-Induced Biomineralization for Accelerated Diabetic Wound Healing*[J]. Advanced Science, 2023. **10**(17).

Preprint of Bio Design and Manufacturing (uncedited)

[16] Yi, L., Y. Ju, Y. He, et al., *Intraperitoneal injection of Desferal® alleviated the age-related bone loss and senescence of bone marrow stromal cells in rats*[J]. Stem Cell Research & Therapy, 2021. **12**(1): p. 45.

[17] Su, N., C. Villicana, C. Zhang, et al., *Aspirin synergizes with mineral particle-coated macroporous scaffolds for bone regeneration through immunomodulation*[J]. Theranostics, 2023. **13**(13): p. 4512-4525.

[18] Liang, C., X. Lin, S.L. Wang, et al., *Osteogenic potential of three different autogenous bone particles harvested during implant surgery*[J]. Oral Dis, 2017. **23**(8): p. 1099-1108.

[19] Ratheesh, G., C. Vaquette and Y. Xiao, *Patient-Specific Bone Particles Bioprinting for Bone Tissue Engineering*[J]. Adv Healthc Mater, 2020. 10.1002/adhm.202001323: p. e2001323.

[20] Otero, L., M. Zurita, C. Bonilla, et al., *Allogeneic bone marrow stromal cell transplantation after cerebral hemorrhage achieves cell transdifferentiation and modulates endogenous neurogenesis*[J]. Cytotherapy, 2012. **14**(1): p. 34-44.

[21] Zhang, G.-W., T.-X. Gu, X.-Y. Guan, et al., *HGF and IGF-1 promote protective effects of allogeneic BMSC transplantation in rabbit model of acute myocardial infarction*[J]. Cell Proliferation, 2015. **48**(6): p. 661-670.

[22] Lu, L., Y. Liu, X. Zhang, et al., *The therapeutic role of bone marrow stem cell local injection in rat experimental periodontitis*[J]. Journal of Oral Rehabilitation, 2019. **47**(S1): p. 73-82.

[23] Świerczek-Lasek, B., L. Tolak, L. Bijoch, et al., *Comparison of muscle regeneration after BMSC-conditioned medium, syngeneic, or allogeneic BMSC injection*[J]. Cells, 2022. **11**(18): p. 2843.

[24] Wu, J., Q. Wang, X. Fu, et al., *Influence of immunogenicity of allogeneic bone marrow mesenchymal stem cells on bone tissue engineering*[J]. Cell Transplantation, 2016. **25**(2): p. 229-242.

[25] Chu, C.-F., S.-H. Mao, V.B.-H. Shyu, et al., *Allogeneic bone-marrow mesenchymal stem cell with moldable cryogel for craniofacial bone regeneration*[J]. Journal of Personalized Medicine, 2021. **11**(12): p. 1326.

[26] Zhang, R., Q. Zhang, Z. Zou, et al., *Curcumin supplementation enhances bone marrow mesenchymal stem cells to promote the anabolism of articular chondrocytes and cartilage repair*[J]. Cell Transplantation, 2021. **30**.

[27] Arthur, A. and S. Gronthos, *Clinical application of bone marrow mesenchymal stem/stromal cells to repair skeletal tissue*[J]. International Journal of Molecular Sciences, 2020. **21**(24): p. 9759.

[28] Zhang, M., J.P. Matinlinna, J.K.H. Tsoi, et al., *Recent developments in biomaterials for long-bone segmental defect reconstruction: a narrative overview*[J]. Journal of Orthopaedic Translation, 2020. **22**: p. 26-33.

[29] Lu, J., C.S. Chamberlain, M.-l. Ji, et al., *Tendon-to-bone healing in a rat extra-articular bone tunnel model: a comparison of fresh autologous bone marrow and bone marrow–derived mesenchymal stem cells*[J]. The American Journal of Sports Medicine, 2019. **47**(11): p. 2729-2736.

[30] Nakahara, K., M. Haga-Tsujimura, K. Sawada, et al., *Single-staged vs. two-staged implant placement using bone ring technique in vertically deficient alveolar ridges – Part 1: histomorphometric and micro-CT analysis*[J]. Clinical Oral Implants Research, 2016. **27**(11): p. 1384-1391.

Preprint of Bio-Design and Manufacturing (unedited)

[31] Woodruff, M.A., C. Lange, J. Reichert, et al., *Bone tissue engineering: from bench to bedside*[J]. Materials Today, 2012. **15**(10): p. 430-435.

[32] Zhu, Q., S. Tang, Y. Zhu, et al., *Exosomes derived from CTF1-modified bone marrow stem cells promote endometrial regeneration and restore fertility*[J]. Frontiers in Bioengineering and Biotechnology, 2022. **10**: p. 868734.

[33] Song, Y., H. Wu, Y. Gao, et al., *Zinc silicate/nano-hydroxyapatite/collagen scaffolds promote angiogenesis and bone regeneration via the p38 MAPK pathway in activated monocytes*[J]. ACS Applied Materials & Interfaces, 2020. **12**(14): p. 16058-16075.

[34] Gabrielyan, A., M. Quade, M. Gelinsky, et al., *IL-11 and soluble VCAM-1 are important components of hypoxia conditioned media and crucial for mesenchymal stromal cells attraction*[J]. Stem Cell Research, 2020. **45**: p. 101814.

Preprint of Bio-Design and Manufacturing (unedited)

Figures

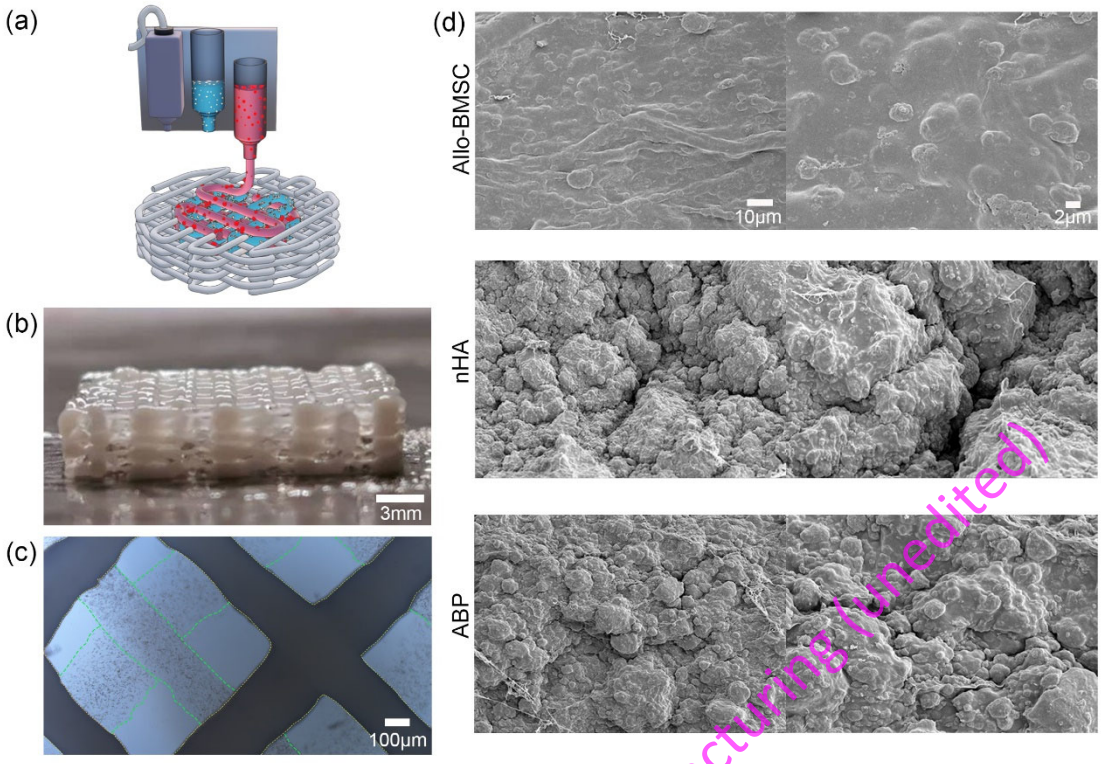

Fig. 1 Morphological characterization of concurrent bioprinted scaffolds. (a) The process of concurrent bioprinting. (b) Photographs of ABP/Allo scaffolds. (c) Images of ABP/Allo scaffolds obtained under an optical microscope (scale bar = 100 μm). The yellow dotted area represents AB bioink, while the green dotted area represents the Allo-BMSCs bioink. (d) Surface morphology images of microfilaments with Allo-BMSCs, ABP, and nHA.

Preprint of Bio-Design and Manufacturing (unedited)

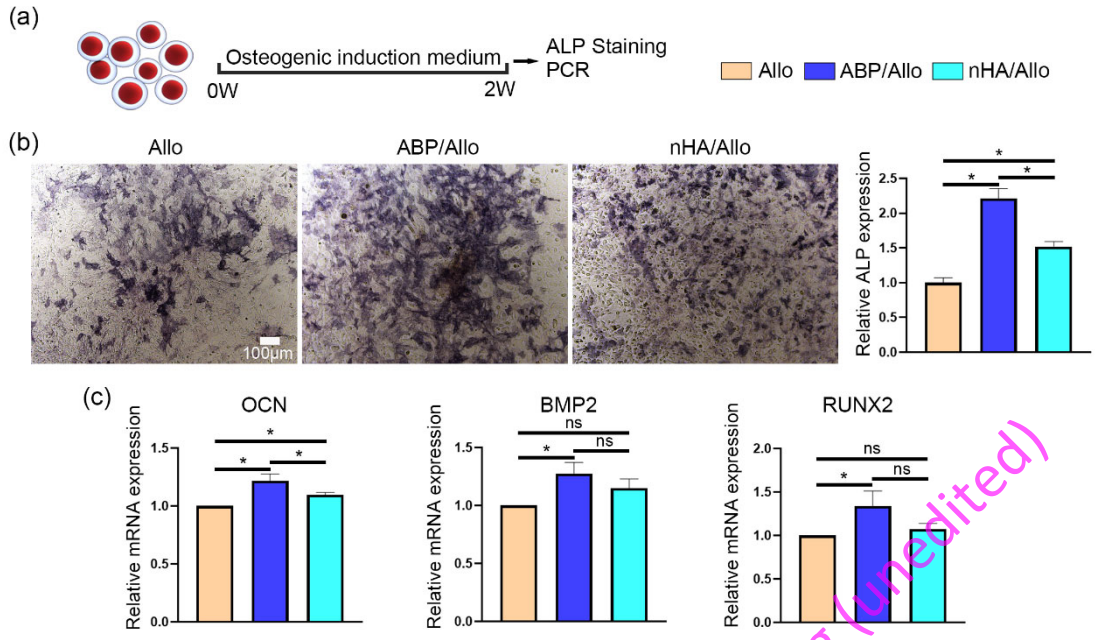

Fig. 2 Osteogenesis evaluation in 2D culture systems *in vitro*.

(a) The experimental design in the *in vitro* 2D culture system. Allo-BMSCs were extracted and cultured in a dish filled with an osteogenic induction medium. After 2 weeks of culturing, cells were prepared for ALP staining and PCR detection. (b) Representative images of ALP staining. The relative ALP expression was evaluated. (c) Relative osteogenesis-related mRNA expression (BMP2, RUNX2, and OCN) were measured. Data are shown as the means ± standard error of the mean, n = 3. * $P < 0.05$, ns. $P \geq 0.05$.

Preprint of Bio-Design and Manufacturing (unedited)

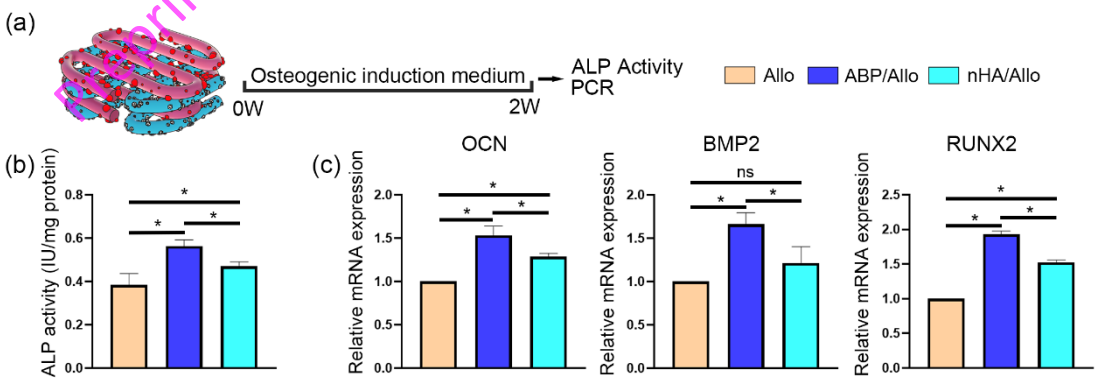

Fig. 3 Osteogenesis evaluation in 3D culture systems *in vitro*.

(a) The experimental design of 3D culture systems. After 3D bio-printing, the scaffolds were

cultured in an osteogenic induction medium for 2 weeks and dissolved in 55 mM trisodium citrate and 20 mM ethylene diamine tetra-acetic acid (EDTA). Finally, the osteogenesis testing was performed by the ALP activity assay and PCR detection. (b) ALP activity of Allo-BMSCs encapsulated in scaffolds was recorded. (c) Relative osteogenesis-related mRNA expression (BMP2, RUNX2, and OCN) was recorded. Data are shown as the means ± standard error of the mean, n = 3. * $P < 0.05$, ns: $P \geq 0.05$.

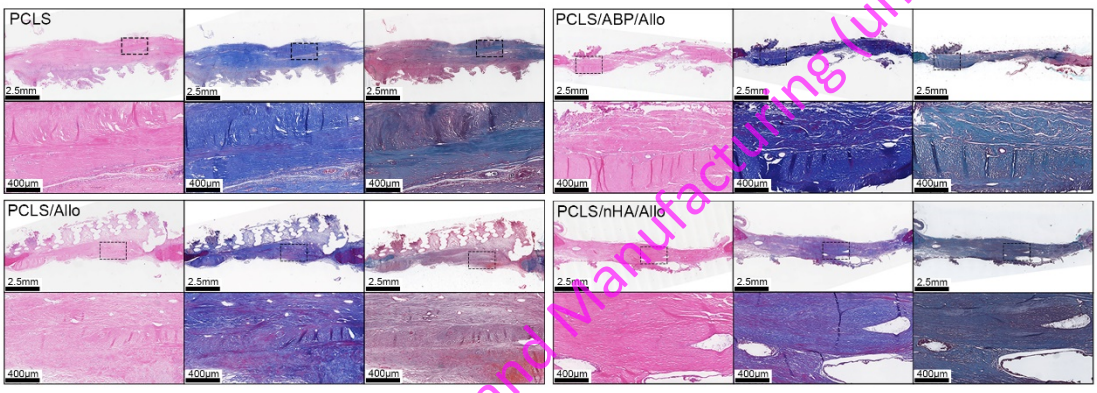

Fig. 4 Histological analysis of bone regeneration 3 months after cranioplasty.

HE, Masson, and Safranin O-Fast Green staining in different groups. The dotted-line area is enlarged below.

Preprint of Bio-Design and Manufacturing (unedited)

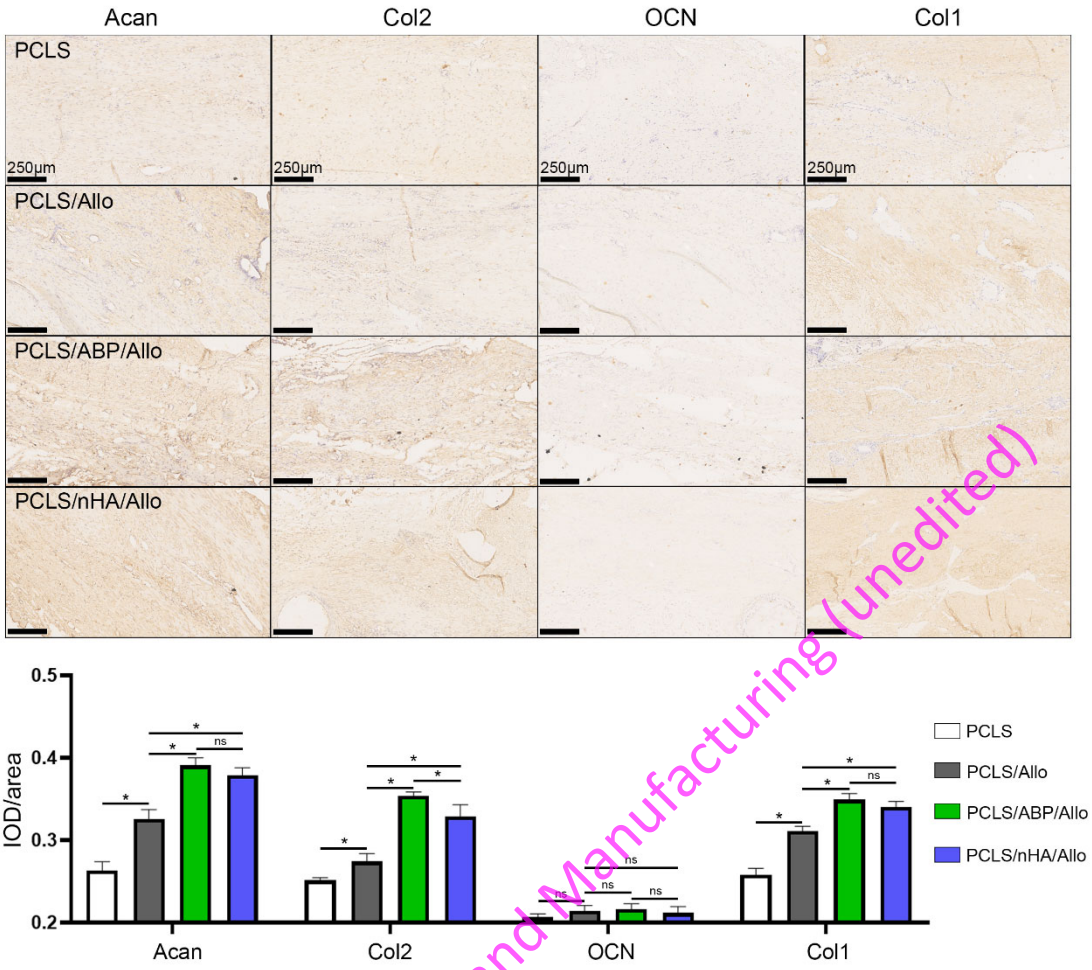

Fig. 5 Immunohistochemistry analysis of bone and cartilage regeneration 3 months after cranioplasty.

Immunohistochemical images of osteogenesis-related proteins including OCN and Col1, chondrogenesis-related proteins including Acan and Col2. The integral optical density per unit area (IOD/area) was recorded. Data are shown as the means ± standard error of the mean, n = 3. *: $P < 0.05$, ns: $P \geq 0.05$.

Preprint of Bio-Design and Manufacturing (unedited)

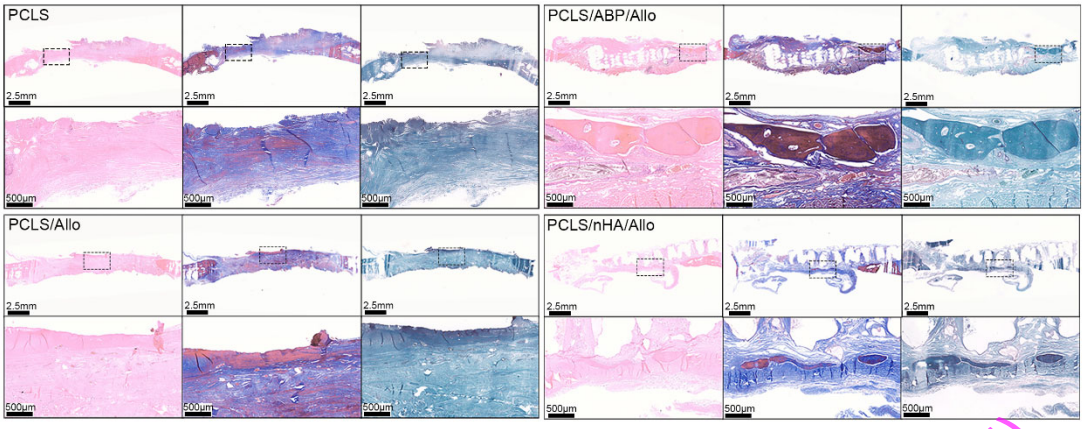

Fig. 6 Histological analysis of bone regeneration 9 months after cranioplasty.

HE, Masson, and Safranin O-Fast Green staining in different groups. The dotted-line area is enlarged below.

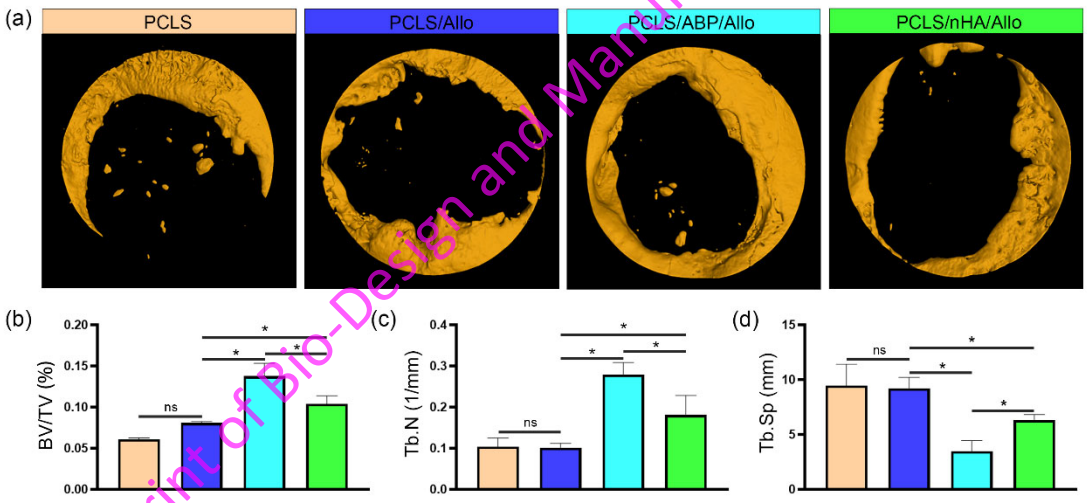

Fig. 7 Micro-CT detection 9 months post-surgery.

(a) Micro-computed tomography (CT) images of cranial defects. (b) The bone volume/total volume (BV/TV) was recorded to evaluate relative bone volume fraction. (c) The number of bone trabecula (Tb.N) and (d) the separation of bone trabecula (Tb.Sp) were recorded. Data are shown as the means ± standard error of the mean, n = 3. *: $P < 0.05$, ns: $P \geq 0.05$.

Preprint of Bio-Design and Manufacturing (unedited)

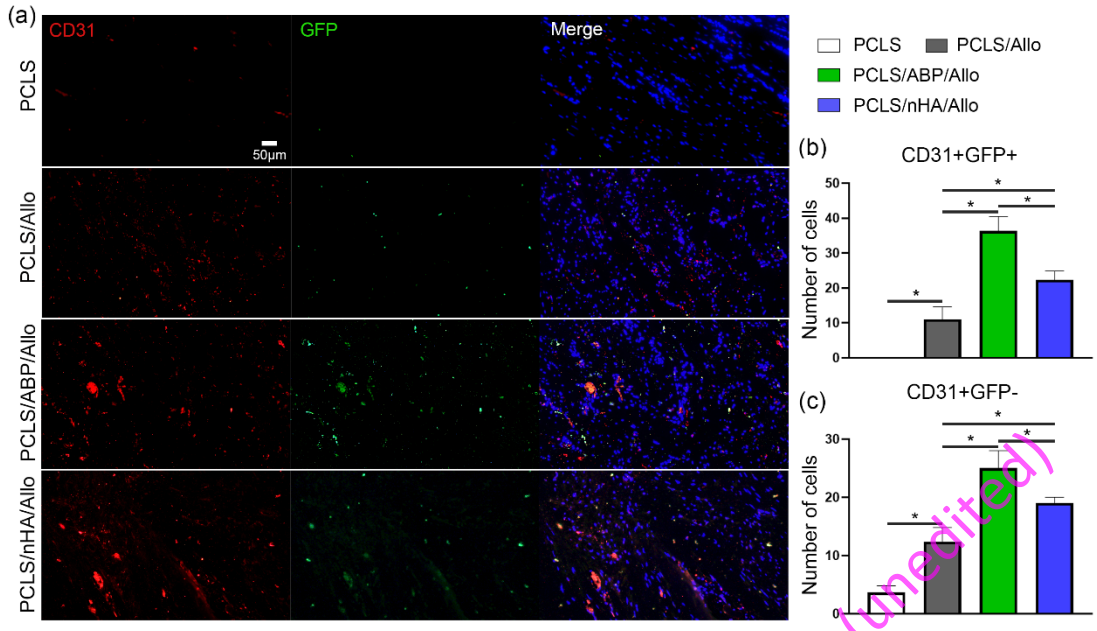

Fig. 8 Evaluation of vascular differentiation of Allo-BMSCs *in vivo*.

(a) Representative images of CD31 and GFP immunofluorescence co-staining. (b) The numbers of CD31+GFP+ and CD31+GFP- cells were recorded. Data are shown as the means ± standard error of the mean, n = 3. *: $P < 0.05$, ns: $P \geq 0.05$.

Preprint of Bio-Design and Manufacturing (unedited)

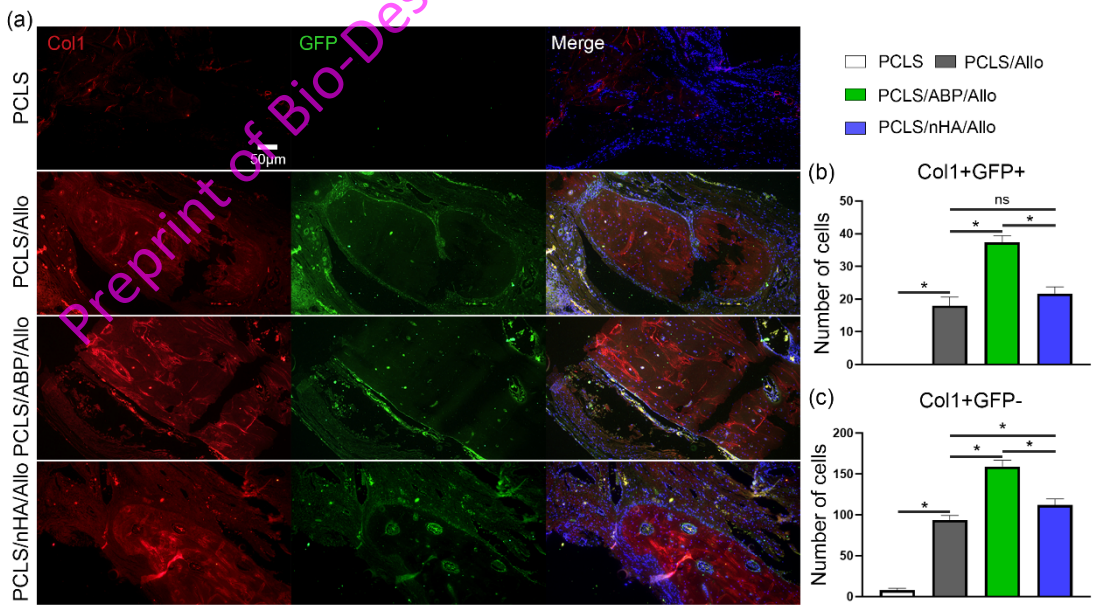

Fig. 9 Evaluation of *in vivo* osteogenic differentiation in Allo-BMSCs.

(a) Representative immunofluorescence images of Col1 and GFP. (b) The numbers of Col1+GFP+

and Col1+GFP- cells were recorded. Data are shown as the means ± standard error of the mean, n = 3. *: $P < 0.05$, ns: $P \geq 0.05$.

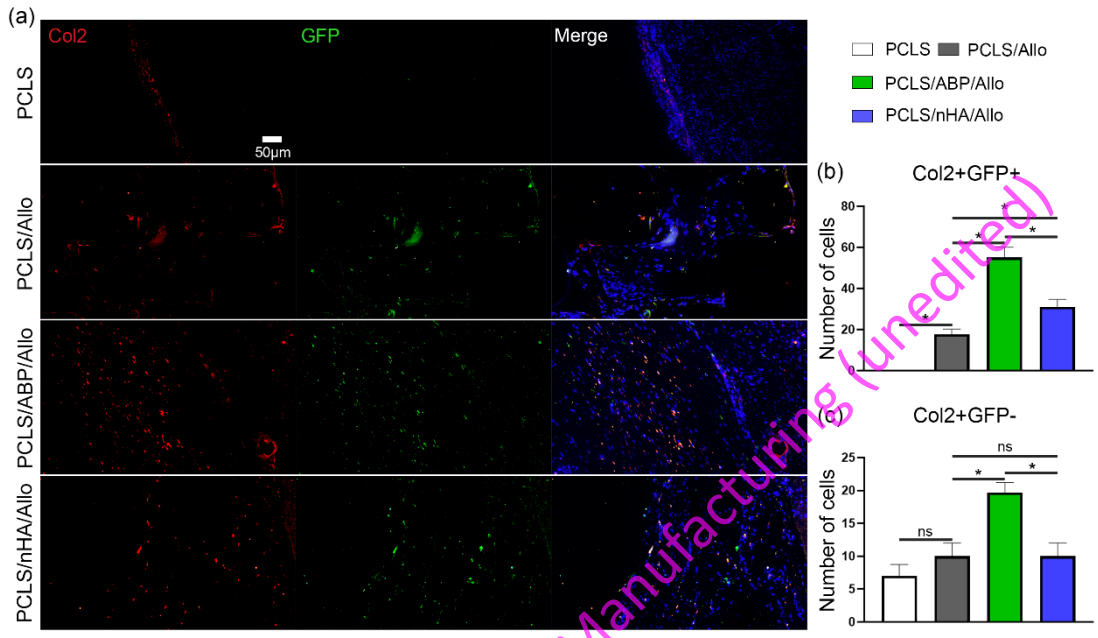

Fig. 10 Evaluation of chondrogenetic differentiation of Allo-BMSCs *in vivo*.

(a) Representative images of Col2 and GFP immunofluorescence staining. (b) The numbers of Col2+GFP+ and Col2+GFP- cells were recorded. Data are shown as the means ± standard error of the mean, n = 3. *: $P < 0.05$, ns: $P \geq 0.05$.

Preprint of Bio-Design and Manufacturing (unedited)

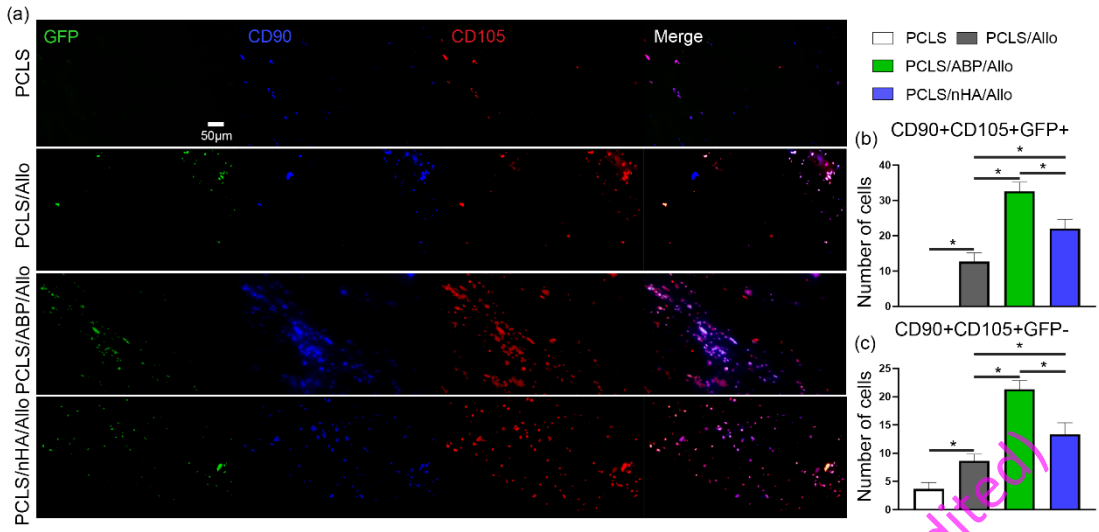

Fig. 11 Evaluation of native BMSCs recruitment *in vivo*.

(a) Immunofluorescence images of CD90, CD105, and GFP co-staining. (b) The numbers of CD90+CD105+GFP+ and CD90+CD105+GFP- cells were recorded. Data are shown as the means ± standard error of the mean, n = 3. *: $P < 0.05$, ns: $P \geq 0.05$.

Preprint of Bio-Design and Manufacturing (unedited)

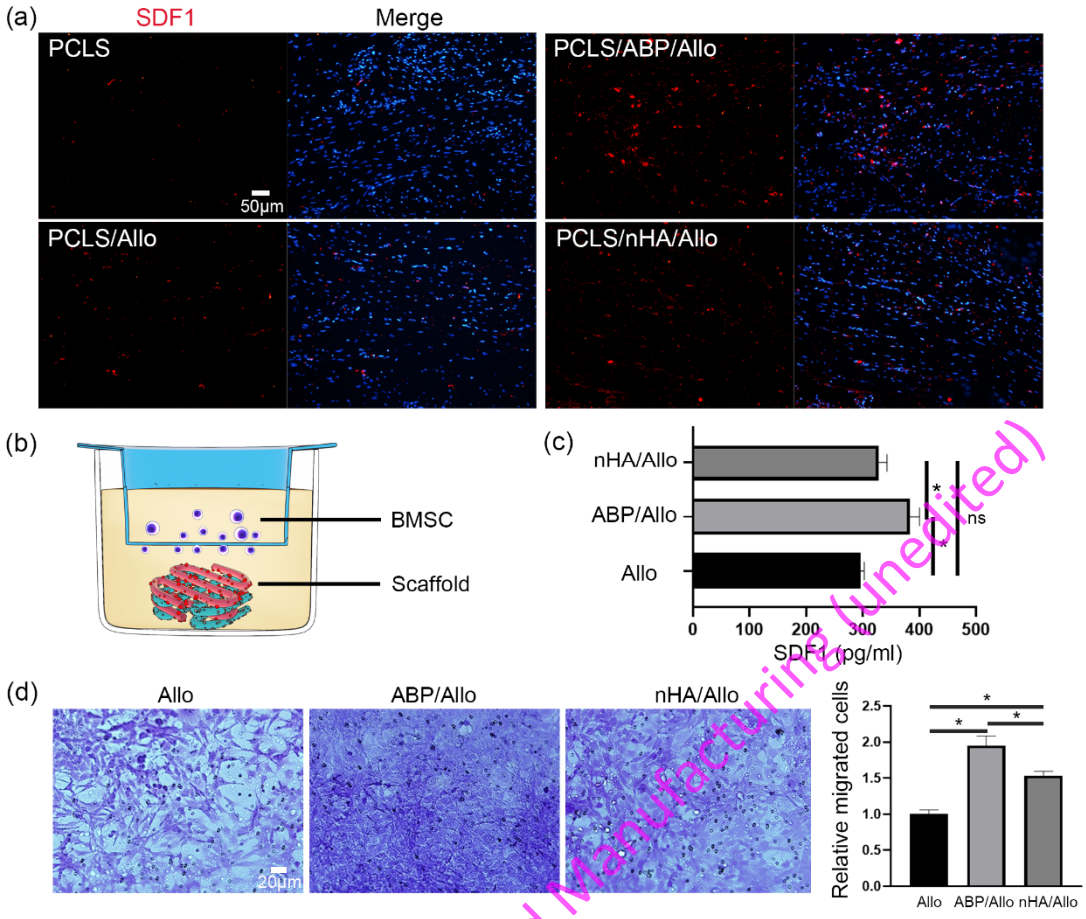

Preprint of Bio-Design and Manufacturing (unedited)

Fig. 12 Evaluation of *in vivo* chemotactic factor expression and native BMSCs recruitment *in vitro*.

(a) Representative images of SDF1 immunofluorescence staining. (b) Schematic diagram of *in vitro* co-culture systems. BMSCs were cultured in the upper transwell chamber for crystal violet coloration detection and SDF1 ELISA, while scaffolds were cultured in the lower transwell chamber. (c) The result of SDF1 ELISA assay in the supernatant of co-culture system was recorded. (d) Crystal violet coloration detection of BMSCs in the upper transwell chamber was performed for BMSC migration, and the relative numbers of migrated cells were recorded. Allo: scaffolds loaded with Allo-BMSCs in the lower chamber; ABP/Allo: autologous bone grafts particles scaffolds loaded with Allo-BMSCs in the lower chamber; nHA/Allo: nHA grafts scaffolds loaded with Allo-BMSCs in the lower chamber. Data are shown as the means ± standard

error of the mean, n = 3. *: $P < 0.05$, ns: $P \geq 0.05$.

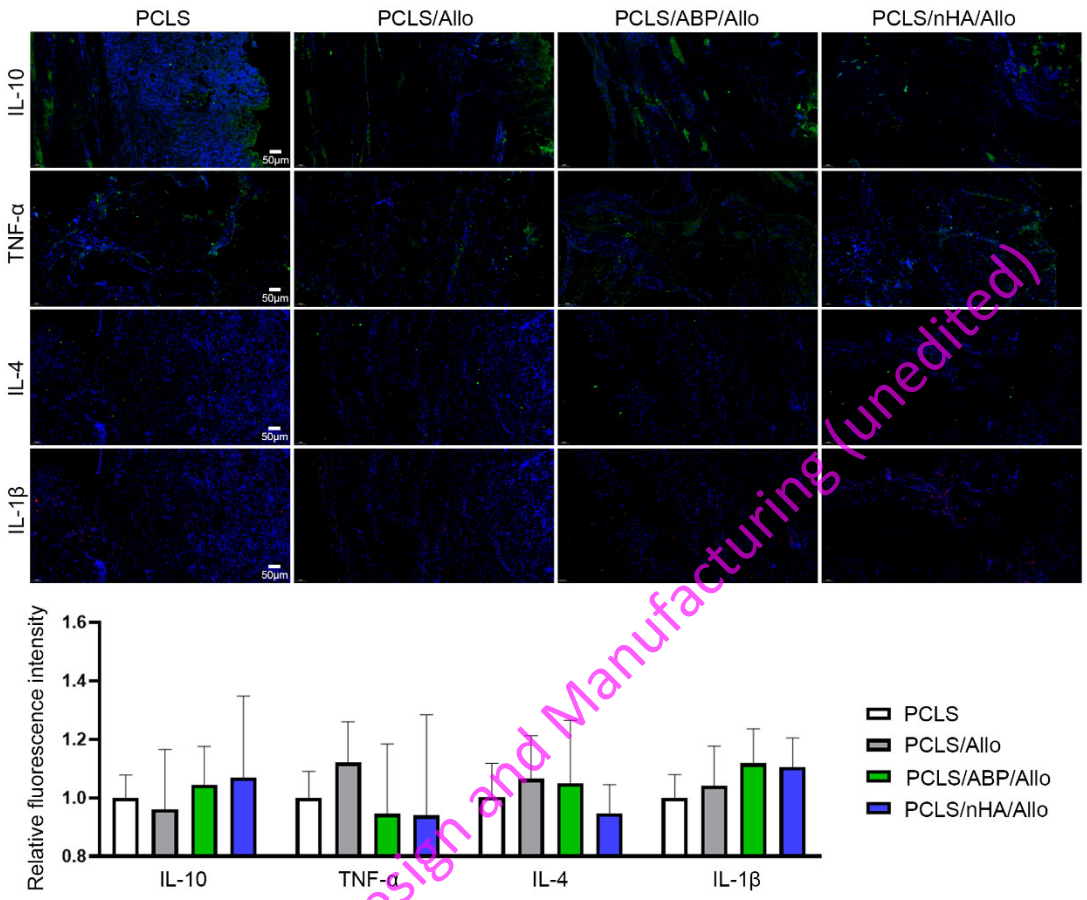

Preprint of Bio-Design and Manufacturing (unedited)

Figure 13. Evaluation of pro-inflammatory and anti-inflammatory cytokines in the lesion site. Representative images of anti-inflammatory cytokines (IL-10, IL-4) and pro-inflammatory cytokines (TNF-α, IL-1β) immunofluorescence were shown. And the relative fluorescence intensity of each group was recorded in which PCLS group was calculated as the control group. The data shown are presented as the mean ± SE (n = 3). *: $P < 0.05$.

Supplemental Figure

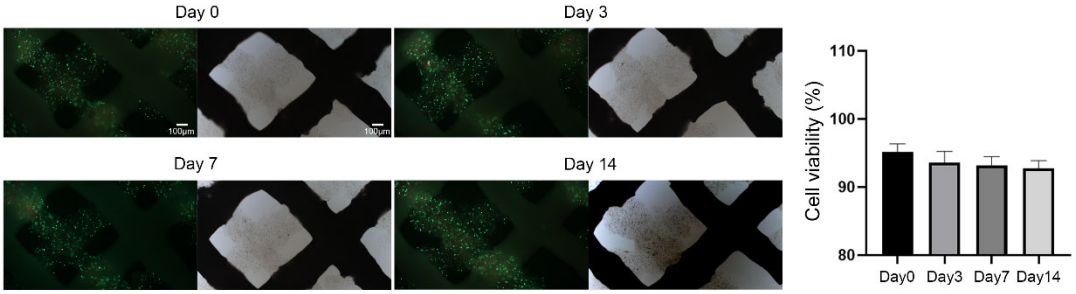

Supplemental Fig. 1 Cell viabilities of ABP/Allo scaffold. Calcein-AM/PI staining (Live/Dead) and bright field images in the different times. The data shown are presented as the mean ± SE (n = 3). *: $P < 0.05$.

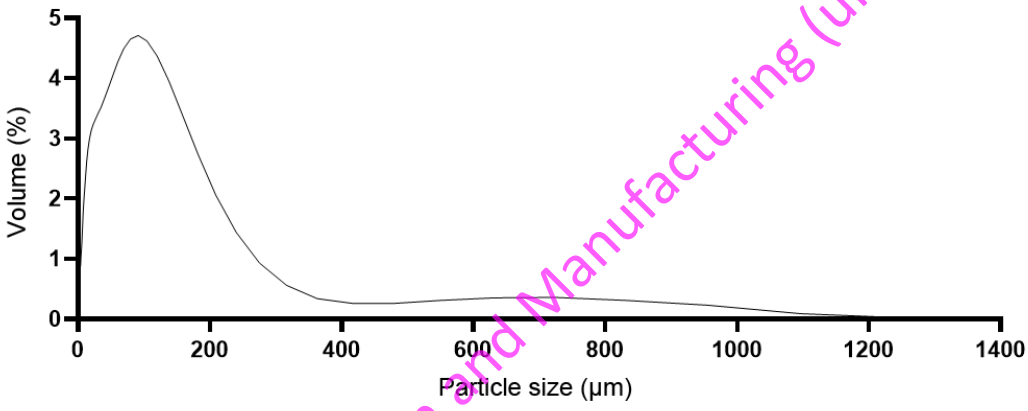

Supplemental Fig. 2 Bone particles size distribution.

Preprint of Bio-Design and Manufacturing (unedited)

Acknowledgments

Not applicable.

Authors' contributions

FF, TX, and ZF designed this study. YH, HQC, and DZZ performed the experiments and completed the analysis. YH and HQC wrote the manuscript. YH, DZZ, and HQC conducted the 3D printing. XH, SZL, BJ, XQW, YND, XWF, and SW provided support in the animal studies. FF, TX, and ZF reviewed and revised the manuscript. All authors read and approved the final

manuscript.

Funding

This study was supported by the Science and Technology Development Fund of Forth Military Medical University (2016XB051), the Military medical promotion plan of Forth Military Medical University (2016TSA-005), the Science and Technology Program of Guangzhou (201604040002), and the Youth Development Project of Air Force Military Medical University (21QNPY072), Xijing Hospital Booster Program（XJZT24CZ10）

Availability of data and materials

The datasets used and analyzed during the current study are available from the corresponding author on reasonable request.

Declarations

All experimental procedures were approved by the Institutional Animal Care and Use Committee of Air Force Military Medical University (No. IACUC-20210120).

Preprint of Bio-Design and Manufacturing (unedited)

Consent for publication

Not applicable.

Competing interests

The authors declare that they have no competing interests.